Rayleigh scattering spectroscopy

Tony F. Heinz

Departments of Physics and Electrical Engineering, Columbia University, New York, NY 10027, USA

Abstract. Single-walled carbon nanotubes can be probed optically by elastic light scattering. This effect forms the basis of a technique, termed Rayleigh scattering spectroscopy, for the study of individual nanotubes. Spectroscopic information on the electronic transitions of both semiconducting and metallic nanotubes is obtained by measuring the elastic scattering cross-section as a function of photon energy. In this chapter, we describe the basic principles of the Rayleigh scattering method and its experimental implementation for rapid and precise measurement of nanotube electronic spectra. The capabilities of the technique are illustrated with several examples of its application. The method offers a natural approach to investigate polarization effects and the persistence of the chiral structure of an individual nanotube, as well as a means to probe nanotube-nanotube interactions. Rayleigh scattering spectroscopy is also well suited for combination with other experimental techniques for the characterization of individual nanotubes. This possibility is illustrated by measurements of Rayleigh spectra of individual nanotubes with chiral indices independently determined by electron diffraction measurements.

1 Introduction

The ability to probe the properties of an *individual* single-walled carbon nanotube (SWNT) using optical spectroscopy is attractive for many investigations. Measurement at the individual nanotube level yields great simplification of the optical spectra. Unlike the situation for ensemble measurements, one is then dealing with just a single, defined nanotube structure. Further, the sensitivity of carbon nanotubes to their local environment can be examined with increased precision when probing individual carbon nanotubes. As discussed elsewhere in this volume, the use of near-field optical techniques can further enhance this sensitivity to the local conditions by providing improvement in spatial resolution compared with that provided by conventional far-field techniques. Optical characterization of individual nanotubes is also of great value in connecting spectroscopic data with information obtained by complementary characterization techniques, such as electron diffraction and transport measurements, that must necessarily be carried out on individual structures.

These compelling motivations for optical spectroscopy at the level of single nanotubes have stimulated researchers to develop several experimental

approaches that provide the required sensitivity. Two purely optical techniques are based on inelastic scattering of photons: photoluminescence spectroscopy [1] and Raman spectroscopy [2,3]. In the former, light is emitted by the lowest-lying excitonic state and the method is limited to semiconducting nanotubes. Using photoluminescence excitation (PLE) spectroscopy, we can also determine the energies of excited states. The Raman technique provides information on the phonon structure of nanotubes. With the aid of the enhancement by electronic resonances, resonance Raman scattering (RRS) can be applied to probe both individual semiconducting and metallic nanotubes. For fixed excitation photon energy, the spectral shifts between the incident and scattered photons provide a map of the accessible vibrational energies. By tuning the incident energy, Raman excitation spectroscopy can provide information about the location of electronic resonances. Both of these methods are extensively discussed elsewhere in the volume. In addition to these purely optical techniques, researchers have recently demonstrated the possibility of obtaining information about the electronic transitions in semiconducting nanotubes by means of the photocurrent spectroscopy for an optically excited nanotube under an electrical bias [4,5].

In this section, we describe an additional experimental approach that has recently been introduced for the spectroscopy of individual single-walled carbon nanotubes [6–9]. The method consists of measurement of the spectral dependence of the cross-section for elastic light scattering. Since the nanotube is an object much smaller than the wavelength of light, this method has been termed Rayleigh scattering spectroscopy. The advantages of the approach include its applicability to both semiconducting and metallic nanotubes, the simple interpretation of the information that the method yields, and the high data collection rate that it can provide at the individual nanotube level. The principal limitation of the method concerns the influence of background scattering and the associated restrictions on the experimental geometry. Through the use of freely suspended nanotubes, this complication can be eliminated.

2 Elastic light scattering

From a fundamental perspective, Rayleigh scattering relies on the same basic optical response as the absorption process, i.e., the linear optical susceptibility χ or dielectric function ϵ of the nanotube. However, since the optical absorption of an individual nanotube is very weak ($< 10^{-4}$ for a tightly focused laser beam), it is more convenient to measure the response in a scattering or dark-field geometry. We can consider the interaction of the nanotube with the incident laser beam as giving rise to an induced dipole moment oscillating at the optical frequency. The radiation emitted in the forward direction interferes with the transmitted optical beam. This corresponds to the absorption process. The strength of the absorption is determined by the imaginary part

of the dielectric function ϵ, since only this phase of the emitted radiation interferes with the transmitted beam.

For Rayleigh scattering, we detect this same dipole emission from the nanotube, but in a background-free direction. Consequently, the scattering signal, which varies as the square of the radiated electric field, scales quadratically with the magnitude of the induced dipole moment, i.e., as $|\epsilon - 1|^2$, where ϵ is the effective dielectric function of the nanotube. By recording the strength of Rayleigh scattering as a function of the frequency of the optical radiation, we obtain a spectrum that reflects the behavior of ϵ as a function of the photon energy. Since electronic transitions in the nanotubes give rise to strong peaks in the dielectric function ϵ, Rayleigh scattering permits ready identification of the electronic transitions in the system.

Before turning to issues involving the signal strength and radiation behavior, we wish to make a brief note about the expected line shape of features in Rayleigh scattering spectroscopy. Unlike absorption measurements, in the scattering configuration the real part of the dielectric function also contributes to the signal strength. While this distinction is of no particular fundamental significance, it is important to bear in mind in considering experimental line shapes. The influence of the real part of the dielectric function can lead to differences in the shape and center of resonances in the Rayleigh spectrum compared with those in an absorption measurement (or any other measurement that scales with absorption, such as photoluminescence excitation spectroscopy). We illustrate this effect in Fig. 1. The Figure shows a series of simulated Rayleigh spectra for a Lorentzian absorption line, but with the inclusion of differing non-resonant (spectrally flat) contributions to the real part of dielectric function ϵ. Such a contribution is present because of the off-resonant electronic transitions. As can be seen from the Figure, despite a fixed behavior for the resonant transitions, there can be significant changes in the observed line shape, as well as a modest shift in the peak of the feature. This effect can easily be incorporated into modeling of the spectral

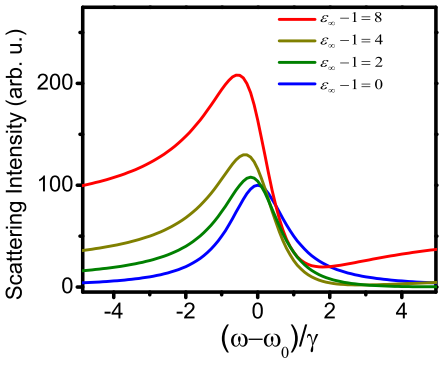

Fig. 1. Simulated line shapes in a Rayleigh scattering measurement, described by $|\epsilon(\omega) - 1|^2$, for a Lorentzian absorption feature. The curves correspond to differing levels of a frequency-independent non-resonant contribution to $\mathrm{Re}(\epsilon)$. $(\omega - \omega_0)/\gamma$ represents the detuning from the resonance at ω_0 in units of the Lorentzian half-width γ. The absorption line shape follows the Rayleigh spectrum for $\epsilon_\infty = 1$.

line shapes, which is necessary for the most precise determination of the line center of a given transition.

To be more quantitative about the radiation process, we describe the elastic light scattering in terms of the interaction of a plane electromagnetic wave with a nanotube. The nanotube is modeled as a long cylinder of diameter d and a relative dielectric function $\epsilon(\omega)$, where ω is the angular frequency of the light. The elastic scattering cross-section per unit length is then given by [10]

$$\sigma_{\rm el}(\omega) = (\pi^2/64)(\omega\, d/c)^3 |\epsilon(\omega) - 1|^2\, d\,, \tag{1}$$

where c denotes the speed of light. We assume here that the polarization of the pump radiation is parallel to the axis of the nanotube and that we are detecting radiation also polarized parallel to the axis. Under these conditions, the emission is isotropic with respect to azimuthal direction and the cross-section includes emission at all angles.

From the expression above, we see that only a relatively low laser power is needed to obtain an adequate elastic scattering rate from an individual nanotube. If we assume, for example, an effective dielectric function of $\epsilon = 6$ for the response of a nanotube of diameter $d = 2\,$nm, we find for Rayleigh scattering of light of wavelength of 500 nm a value of $\sigma_{\rm el} = 1.2 \times 10^{-7}\,\mu$m. For a source with a power of, say, $100\,\mu$W focused to a width of $1\,\mu$m, we then produce scattered photons at a rate of 3×10^7/s. Allowing for an overall collection and detector quantum efficiency of 10^{-2}, this yields a count rate of $\sim 10^5 - 10^6$/s. Such a signal level clearly permits rapid data acquisition for scattering by an individual SWNT.

3 Experimental technique

Figure 2 shows a schematic representation of the dark-field configuration appropriate for Rayleigh scattering spectroscopy. To optimize the signal, one naturally wishes to achieve both tight focusing of the pump laser beam and collection of a large solid angle of the elastically scattered light. This can be accomplished with a pair of matched microscope objectives, with the detection direction arranged to exclude any transmitted laser radiation.

Two distinctive features were incorporated into the initial experimental demonstration of the Rayleigh technique that allowed it to provide high-quality spectra with very short data acquisition times. The first was probing freely-suspended nanotubes, an arrangement for which there was no background scattering of light; the second was the use of a laser-based supercontinuum source that permitted spectra to be collected in parallel over a wide range of wavelengths.

Samples of freely-suspended nanotubes for the Rayleigh scattering measurements are prepared by means of chemical vapor deposition (CVD)on a

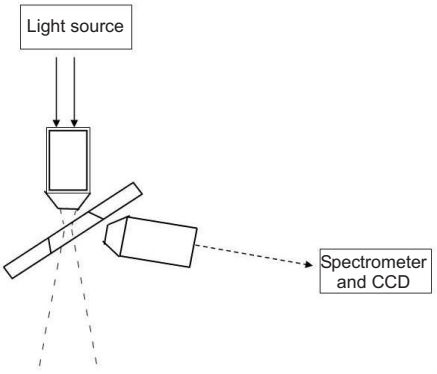

Fig. 2. Schematic diagram for a Rayleigh scattering measurement. Microscope objectives focus the incident light on a suspended nanotube and collect the radiation scattered light. Using a super-continuum source, we can detect different wavelengths simultaneously with a spectrometer and multi-channel (CCD) camera.

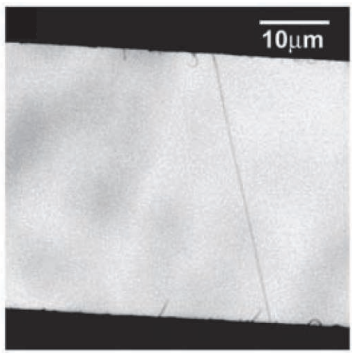

Fig. 3. Electron micrograph of an individual suspended SWNT. The sample is prepared by CVD using a substrate with a slit etched in it. Typical slit widths are 10's of microns and slit lengths are up to 1 mm. (After Ref. [6].)

silicon substrate into which a completely open slit has been etched by standard microfabrication techniques. Figure 3 shows an electron microscope image of an individual suspended SWNT crossing such a slit. The width of the slit can be varied depending on experimental requirements, but is typically chosen in the range of 10's of microns to ensure that there is no appreciable scattering from accidental illumination of the substrate by stray pump light. The length of the slit (perpendicular to the nanotubes) can be as great as 1 mm, so that a single substrate can provide many individual SWNTs for study. By scanning the position of the sample relative to the probe beam, one can access different nanotubes or a given nanotube at different positions along its axis.

The preparation of the samples does not require any delicate manipulation of the nanotubes make them bridge the slit. In the CVD growth, one simply places an appropriate metal catalyst for nanotube growth on the substrate at a distance from the slit. The nanotubes are then grown with the reactor gas flow directed from the catalyst towards the slit. As the nanotubes grow, they follow reactor gas stream, remaining above the substrate. When the gas flow ceases, the nanotubes fall onto the substrate and, if sufficiently long, spontaneous cross the slit. Samples have been prepared using several distinct catalysts, such as Fe and Co thin films, and various feedstock gases, such as ethanol and methane [11,12]. Adjustments of the feedstock gases and catalyst are made to ensure that the nanotubes are sufficiently sparse in the region of the slit so that only one SWNT will normally fall within the spot size

($\sim 1\,\mu$m) of the focused optical pump radiation. That this condition is met can be verified by the characteristics of the observed Rayleigh spectrum. One can thus perform single nanotube spectroscopy without the complexity of near-field optical techniques. Of course, the spatial resolution along the nanotube is limited to the size of the focused pump beam. As discussed elsewhere in this volume, near-field methods can significantly improve upon this longitudinal resolution.

The second experimental feature that facilitates collection of Rayleigh scattering spectra is the use of an optimized light source for the measurement. To obtain useful spectroscopic information from Rayleigh scattering, we must scan the wavelength of the light undergoing scattering. This can certainly be accomplished by means of a tunable laser source, as is done for photoluminescence excitation spectroscopy or Raman excitation spectroscopy at the single nanotube level. This process is, however, relatively slow and somewhat tedious when one wishes to cover a broad spectral range. Since the power needed to observe the elastically scattered light is low, researchers have shown the possibility of making use of a broadband laser-based source for the *simultaneous* measurement of Rayleigh scattering over a range of wavelengths. With an appropriate high-brightness broadband source, one can use parallel, multi-channel detection to obtain the entire (excitation) spectrum at once. It should be noted that this method implicitly assumes that the strength of elastically scattered light dominates inelastic contributions. This is a very good approximation for the concurrent Raman scattering process, since the vibrational coupling is weak and Raman scattering is inefficient compared with the elastic light scattering. The only condition under which one must exercise some care would be for detection in the vicinity of the E_{11} transition in semiconducting nanotubes where fluorescent emission may be strong enough to compete with elastic scattering.

Bright continuum radiation with a spectrum extending from photon energies below 1 eV to approximately 3 eV can be obtained by passing femtosecond modelocked laser pulses through an optimized nonlinear fiber [13]. Such sources may either be constructed in the laboratory from standard modelocked oscillators or purchased as integrated commercial units. In either case, the radiation emerges from an optical fiber, which facilities its efficient focusing by a microscope objective. A suitable level of optical radiation for the Rayleigh spectroscopy measurements is typically a fraction of a milliWatt of optical power. Such focused continuum radiation provides a reasonable level for the Rayleigh scattering signal without significant heating of the nanotube. As for the precision of the measured spectra, this is controlled entirely by the arrangement of the multi-channel detection scheme, i.e., by the dispersion of the spectrometer and the number of channels of the detector. For a suitable choice of grating dispersion, spectra resolution of a few meV can be achieved over a broad energy range using a standard CCD camera. This resolution fully resolves the features of electronic transitions of SWNTs, particularly for the

higher E_{nn} transitions, which exhibit increased widths compared with the E_{11} transition.

Figure 4 displays results of Rayleigh scattering from several individual semiconducting and metallic SWNTs. The observed transitions are the E_{33} and E_{44} for the semiconducting nanotubes and the M_{11} for the metallic nanotubes. Note in Fig. 4 (d), the two traces for the (10,10) nanotubes. These are data from two completely separate measurements of different individual SWNTs. The high level of reproducibility of the measurements is apparent.

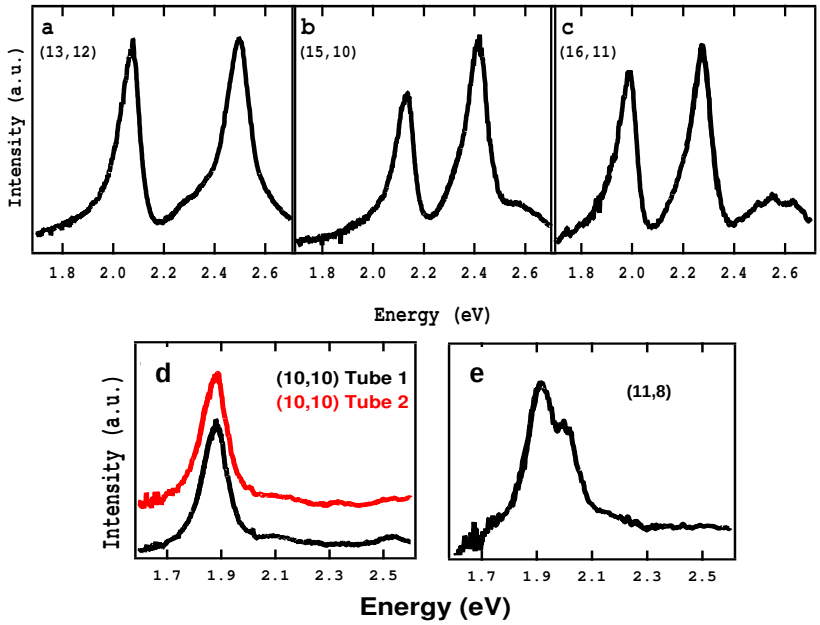

Fig. 4. Experimental Rayleigh scattering spectra for individual SWNTs of the specified chiral indices. The nanotubes (a) - (c) are different semiconducting structures; those of (d) and (e) are metallic nanotubes. The two sets of data for the (10,10) structure (displaced for clarity) correspond to completely independent measurements of different nanotubes. The chiral indices of all of the nanotubes were determined independently by electronic diffraction. (After Ref. [7].)

4 Application of the technique

Despite the relatively recent introduction of the method of Rayleigh scattering spectroscopy, the approach has already provided several interesting results about the optical properties and interactions of SWNTs [6–9]. Here we review some representative studies to illustrate the capabilities of this method for single nanotube spectroscopy.

4.1 Electronic transitions of nanotubes of independently determined structure

Figure 4 illustrates the capability of Rayleigh spectroscopy to provide high-quality spectra of individual SWNTs. The spectra are taken under favorable conditions in terms of having nanotubes unaffected by their environment, since the nanotubes are well isolated from one another and suspended in air. The spectra of the electronic transitions thus provide an attractive point for a rigorous comparison with theory. To do so, however, we have to overcome a fundamental limitation in a purely optical measurement, namely, that we do not have direct and independent knowledge of the structure of the material under study. Once appropriate assignments of spectroscopic features have been made, optical measurements can, of course, yield such structural information. Such careful assignments have been made of the optical transitions in ensemble samples containing nanotubes of various chiral indices using predicted theoretical trends and a wealth of experimental data [14].

Since accurate calculations of the transition energies, particularly for large- diameter or low-symmetry nanotubes, remain difficult, there is a motivation to obtain transition energies of individual nanotubes whose structure

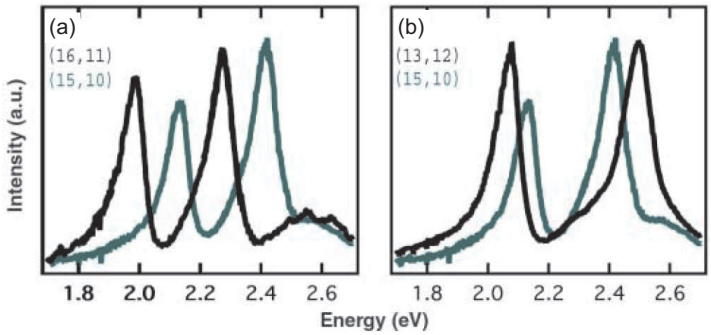

Fig. 5. Comparison of Rayleigh scattering spectra of similar semiconducting nanotubes from the data in Fig. 4 (a-c). The peaks correspond to the E_{33} and E_{44} transitions. The comparison in (a) corresponds to two nanotubes in the same $(2n+m)$mod3 type, but different diameters; The comparison (b) involves two nanotubes of different $(2n+m)$mod3 type, but with similar diameters. (After Ref. [7].)

has been determined independently of any spectroscopic analysis. This goal has been met by combining the Rayleigh scattering data with direct structural analysis by electron diffraction at the individual nanotube level. The diffraction data provide an unambiguous structural assignment of individual nanotubes with optical spectra previously measured by Rayleigh scattering spectroscopy. In Fig 4, the indicated chiral indices have been obtained from such analysis by electron diffraction [7]. We note that an analogous study was recently performed in which electron diffraction of individual carbon nanotubes was combined with single-nanotube Raman spectroscopy to obtain definitive information on the frequencies of Raman features for nanotubes of known structure [15].

A detailed comparison of the Rayleigh spectra for semiconducting nanotubes in Fig. 4 (a-c) is instructive. In Fig. 5, we show the Rayleigh spectrum of the (15,10) nanotube in comparison with the (16,11) nanotube in the left panel and with the (13,12) nanotube in the right panel.

For the case of the (16,11) nanotube, we have a structure with the same of $(2n + m)\mathrm{mod}3 = 1$ value (type I) as the (15,10) reference nanotube. The diameter of the (16,11) nanotube of 1.83 nm is 0.12 nm greater than the 1.71 nm diameter of the (15,10) nanotube. We consequently see a significant shift (of about 150 meV) towards lower energies in the transitions of the larger (16,11) nanotube. The ratio of the E_{44} to E_{33} transition energies is, however, quite similar – 1.150 for the larger (16,11) nanotube versus 1.135 for the smaller (15,10) nanotube – for these two nanotubes of the same type.

A comparison of the (13,12) nanotube with the (15,10) reference nanotube shows different behavior. In this case, the average energies of the two transitions of the (15,10) and (13,12) nanotubes are very similar, differing only by ~ 10 meV. This might be anticipated given the nearly identical respective diameters of 1.71 nm and 1.70 nm for the two nanotubes. For this pair of nanotubes, however, the (13,12) nanotube is a type II ($(2n + m)\mathrm{mod}3 = 2$) structure, while the reference (15,10) nanotube is type I. This difference is manifested in dissimilar ratios of the E_{44} to E_{33} transition energies: 1.206 versus 1.135 for the (13,12) and (15,10) chiral indices, respectively. While the numerical values differ from those predicted by simple tight-binding models [16], the trend is exactly as predicted for nanotubes of type I and type II structure. Detailed examination of the Rayleigh data also permitted confirmation of the predicted trends for different chiral angles [7].

4.2 Polarization dependence of nanotube electronic transitions

In any ensemble optical measurement of nanotubes, the measurement necessarily averages over a variety of angular orientations of the nanotube. This severely complicates the study of the polarization properties of the optical transitions, which can be addressed only through achieving partial orientation of the nanotubes [17] or through measurements involving two distinct electronic transitions [18]. At the single nanotube level, these complexities

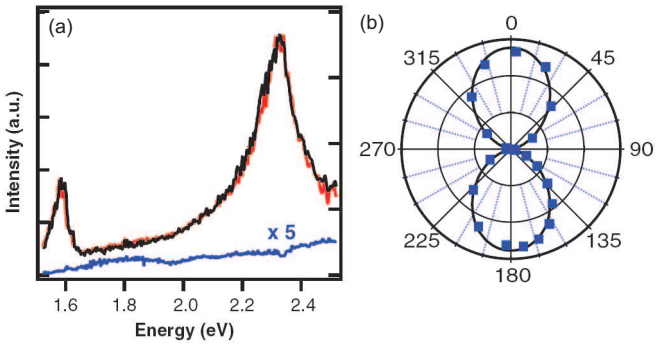

Fig. 6. Polarization effects observed in the Rayleigh spectrum on an individual SWNT. The polar plot (b) shows the nearly dipole dependence of the Rayleigh scattering on the polarization of the probe beam. The spectrum (a) displays the response parallel (large) and perpendicular (small) to the nanotube axis. The parallel spectrum is comprised of two traces, obtained at a separation of 30 μm from one another along the nanotube axis, a result indicating that no structural change occurs. (After Ref. [6].)

disappear. Figure 6 presents an example of the strong polarization effects for the optical transitions in SWNTs manifested in Rayleigh scattering spectra. The local-field or antenna effect strongly reduces the response when the electric-field vector of the optical radiation lies perpendicular to the nanotube axis [19]. Indeed, the response is essentially that of a dipole ($\cos 2\theta$) intensity pattern, as shown in Fig. 6 (b). Close inspection of the spectra for excitation along and perpendicular to the nanotube axis reveals, however, the existence of a weak, but measurable response from the perpendicular configuration. This response arises from electronic transitions of the type $E_{n,n-1}$ and $E_{n-1,n}$ [18] that contribute to optical response perpendicular to the nanotube axis. The electromagnetic screening mentioned above, however, sharply reduces the observed strength of these transitions, particularly when an electronic resonance is approached.

4.3 Structural stability along the nanotube axis

The ability to grow long nanotubes by chemical vapor deposition combined with the possibility of rapid characterization of the electronic transitions (and, hence, physical structure) of the nanotubes permits study of the structural stability of the nanotube. Analysis of many CVD-grown nanotubes has shown that changes in chiral index are infrequent, with most nanotubes of lengths of 10's of microns showing no change in structure. A representative set of data is shown in Fig. 6 (a). Here precisely the same Rayleigh spectrum (and, hence, same nanotube structure) is observed at a displacement of 30 μm along an individual SWNT.

Because of its rapid data collection rate, Rayleigh spectroscopy allows convenient characterization of large numbers of nanotubes. This has permitted the identification of infrequent spontaneous changes of the chiral index of a nanotube along its axis to be identified and the site of this structural transformation determined to optical resolution. A method has also been introduced that permits suspended nanotubes to be transferred onto a solid substrate at a desired location [20]. With the aid of this technique, one can first characterize the nanotube by Rayleigh spectroscopy and then place it in a convenient location for complementary additional characterization. Initial experiments of this type have been performed in which the electrical transport properties of optically characterized nanotubes have been determined [9].

4.4 Nanotube-nanotube interactions

The ability to probe individual nanotubes provides a controlled approach for the investigation of the effect of the environment on nanotube properties. Since SWNTs are only one monolayer in thickness, one expects that the effect of the external environment can be significant. Such interactions are, of course, quite diverse in character, ranging from chemical modification to physical deformation.

Figure 7 illustrates the use of Rayleigh scattering spectroscopy to probe one class of change induced by the local environment [8]. In this case, we are able to probe an individual SWNT in its isolated form and as a part of a bundle with a second SWNT. This structure was formed spontaneously in the CVD growth process. One nanotube extended fully across the slit, while a second nanotube formed a bundle over half the width of the slit. The Rayleigh spectra of the isolated nanotube (A) and of the bundled structure (A+B) are shown. In the bundle, one can clearly identify the peaks associated with nanotube (A), in addition to new features arising from electronic transitions

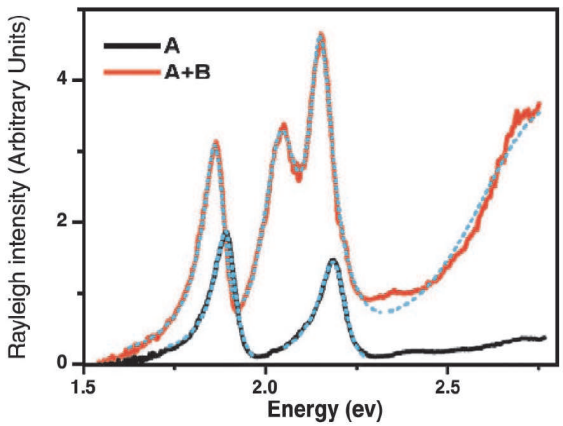

Fig. 7. Rayleigh spectra of an isolated nanotube (A) and of a bundle consisting of nanotube A and a second nanotube (A+B). The peaks of nanotube A can be seen in the bundle, together with additional peaks from nanotube B. The peaks of nanotube A are shifted to the red by 10's of meV when they appear in the bundle. (After Ref. [8].)

in nanotube (B). The noteworthy feature in the spectra is that the transitions in nanotube A (the E_{33} and E_{44} transitions in a semiconducting nanotube) are clearly shifted in energy when they appear in the two-nanotube bundle. The peaks are displaced to lower energy by 10's of meV when an adjacent nanotube is present in a bundle. In other data sets for similar configurations, the shifts are consistently to lower energy upon bundling. In addition, in some cases the nanotubes form spontaneously form Y-junctions. It is then possible to measure the spectra of each of the two isolated constituents of the bundle separately and to determine the shifts undergone by each component in forming the bundle [8]. Again, we see red shifts for all transition energies. This observation suggests that possible strain effects are not significant, since the influence of strain would generally push some transition energies up and some down.

We can understand a red-shift induced by bundling as a consequence of dielectric screening of the strong carrier-carrier interactions in a nanotube. The presence of an adjacent dielectric medium (nanotube B in Fig. 7) reduces the carrier-carrier interactions within the nanotube being probed (nanotube A in Fig. 7). The importance such carrier-carrier interactions has been predicted theoretically by several researchers [21–26] established experimentally by observation of strong excitonic effects in semiconducting nanotubes [27–29]. Screening of this carrier-carrier interaction leads to a reduced quasi-particle band gap (because of decreased electron-electron repulsion). Although this effect is partially offset by a reduced exciton binding energy, the net shift in the transition energy of the exciton caused by the dielectric screening is expected to be towards lower energy. Spectral shifts of nanotube transitions from bundling and other environmental effects have been widely reported in previous ensemble measurements [30,31]. As shown here, access to optical measurements at the single nanotube level permits these interesting phenomena to be examined with a degree of control difficult to match in an ensemble measurement.

5 Outlook

Elastic light scattering from individual nanotubes is strong enough to be readily observed in the absence of background signals. Spectroscopy of the electronic transitions in nanotubes can thus be obtained by measuring the cross-section for elastic scattering as a function of the photon energy, which provides direct information on the linear optical properties of the nanotube under study. The resulting technique of Rayleigh scattering spectroscopy, when applied with a continuum light source, allows for rapid and precise measurement of the optical transitions in individual SWNTs of both semiconducting and metallic character.

The principal limitation in application of the method of Rayleigh scattering spectroscopy is, in some sense, the counterpoint of its strength. All types

of nanotubes provide an elastic light-scattering response, making the method applicable to metallic, as well as semiconducting nanotubes, small bundles, and nanotubes with high defect densities, and so on. By the same token, however, any material other than the nanotube that is illuminated by the probe beam can also yield elastically scattered light, radiation that may be difficult to separate from the nanotube signal. By probing nanotubes suspended in air, this complication is eliminated. However, for a more general sample geometry, the role of background scattering must be considered, since such background signals can be far stronger than the nanotube response. While the distinctive spectral and polarization characteristics of the nanotube response can be identified in the presence of a spectrally unstructured background, this becomes difficult if the relative strength of the background signal is too great compared with the signal of interest. It should be noted, however, that an ideal planar surface does not give rise to diffuse scattering and would thus be compatible with Rayleigh scattering measurements from individual SWNTs. Understanding the practical limitations of the method in such cases and perhaps developing suitable spatial, spectral, or polarization modulation techniques to discriminate against undesired background signals is an interesting area for future development.

Rayleigh scattering spectroscopy provides a useful addition to the established techniques of Raman and photoluminescence spectroscopy that are based on inelastic light scattering. While all three of the methods permit access to spectroscopy of individual SWNTs, the methods are largely complementary to one another. Rayleigh spectroscopy is extends photoluminescence measurements in its applicability to all nanotubes, including metallic species and semiconducting nanotubes for which fluorescence emission is weak (high level of defects) or difficult to detect (at long wavelengths). Rayleigh spectroscopy is also complementary to Raman and photoluminescence measurements in its ability to provide broad-band excitation spectra rapidly at the single nanotube level. This attribute makes it particularly convenient to combine Rayleigh and Raman spectroscopy for the study of individual SWNTs. By performing the Rayleigh spectroscopy first, one obtains information to ensure a choice of laser photon energy that benefits from the desired resonant enhancement of the Raman process. Further, the usual instrumentation for Rayleigh scattering serves for Raman (or photoluminescence) measurements simply by replacing the continuum source with the appropriate monochromatic laser excitation. Beyond the experimental convenience of performing Rayleigh and Raman spectroscopy jointly, the information from the two measurements, electronic and vibrational spectra, are complementary and together provide a very complete characterization of any nanotube under study.

In addition to combining Rayleigh scattering with other single nanotube optical spectroscopies, Rayleigh spectroscopy can be fruitfully used, as illustrated in our earlier discussion of electron diffraction, in conjunction with

entirely different experimental methods. This direction, while not unique to the Rayleigh scattering technique, will certainly become increasingly important in the future. From this perspective, Rayleigh scattering is attractive because of its short measurement time and its applicability to all types of nanotubes. A further frontier for measurements of individual nanotubes is accessing dynamics directly in the time domain. Impressive results have been demonstrated in time-resolved photoluminescence at the individual nanotube level [32]. To expand these measurements to a range of pump-probe techniques with the full femtosecond time resolution of current laser techniques requires a sensitive probe of the response of individual SWNTs. Rayleigh scattering, with its high signal strength, appears to be a promising optical probe for such measurements.

The author would like to thank M. Dresselhaus, J. Maultzsch, and Y. Wu for helpful discussion in preparing this chapter and acknowledge support from the Nanoscale Science and Engineering Initiative of the U.S. National Science Foundation under grants CHE-0117752 and ECS-05-07111, the New York State Office of Science, Technology, and Academic Research (NYSTAR), and the Office of Basic Energy Sciences, U.S. Department of Energy under grant DE-FG02-03ER15463.

References

1. A. Hartschuh, H. N. Pedrosa, J. Peterson, L. Huang, P. Anger, H. Qian, A. J. Meixner, M. Steiner, L. Novotny, and T. D. Krauss, Chem. Phys. Chem. **6**, 577 (2005).
2. M. S. Dresselhaus, G. Dresselhaus, A. Jorio, A. G. Souza-Filho, G. G. Samsonidze, and R. Saito, J. Nanosci. Nanotech. **3**, 19 (2003).
3. M. S. Dresselhaus, G. Dresselhaus, R. Saito, and A. Jorio, Physics Reports **409**, 47 (2005).
4. J. U. Lee, P. J. Codella, and M. Pietrzykowski, Appl. Phys. Lett. **90**, 053103 (2007).
5. X. Qiu, M. Freitag, V. Perebeinos, and P. Avouris, Nano Lett. **5**, 749 (2005).
6. M. Y. Sfeir, F. Wang, L. Huang, C.-C. Chuang, J. Hone, S. P. O'Brien, T. F. Heinz, and L. E. Brus, Science **306**, 1540 (2004).
7. M. Y. Sfeir, T. Beetz, F. Wang, L. Huang, X. M. H. Huang, M. Huang, J. Hone, S. O'Brien, J. A. Misewich, T. F. Heinz, L. Wu, Y. Zhu, *et al.*, Science **312**, 554 (2006).
8. F. Wang, M. Y. Sfeir, L. Huang, X. M. H. Huang, Y. Wu, J. Kim, J. Hone, S. O'Brien, L. E. Brus, and T. Heinz, Phys. Rev. Lett. **96**, 167401 (2006).
9. B. Chandra, R. Caldwell, M. Huang, L. Huang, M. Y. Sfeir, S. P. O'Brien, T. F. Heinz, and J. Hone, phys. stat. sol. (b) **243**, 3359 (2006).
10. C. F. Bohren and D. R. Huffman, *Absorption and Scattering of Light by Small Particles* (Wiley, New York, 1983).
11. L. Huang, S. Wind, and S. P. O'Brien, Nano Lett. **3**, 299 (2003).
12. L. Huang, X. Cui, B. White, and S. P. O'Brien, J. Phys. Chem. B **108**, 16451 (2004).

13. J. M. Dudley, G. Genty, and S. Coen, Rev. Mod. Phys. **78**, 1135 (2006).
14. S. M. Bachilo, M. S. Strano, C. Kittrell, R. H. Hauge, R. E. Smalley, and R. B. Weisman, Science **298**, 2361 (2002).
15. J. C. Meyer, M. Paillet, T. Michel, A. Moréac, A. Neumann, G. S. Duesberg, S. Roth, and J.-L. Sauvajol, Phys. Rev. Lett. **95**, 217401 (2005).
16. R. Saito, G. Dresselhaus, and M. S. Dresselhaus, *Physical Properties of Carbon Nanotubes* (Imperial, London, 1998).
17. M. F. Islam, D. E. Milkie, C. L. Kane, A. Yodh, and J. Kikkawa, Phys. Rev. Lett. **93**, 037404 (2004).
18. Y. Miyauchi, M. Oba, and S. Maruyama, Phys. Rev. B **74**, 205440 (2006).
19. H. Ajiki and T. Ando, Physica B **201**, 349 (1994).
20. X. M. H. Huang, R. Caldwell, L. Huang, S. C. Jun, M. Huang, M. Y. Sfeir, S. P. O'Brien, and J. Hone, Nano Lett. **5**, 1515 (2005).
21. T. Ando, J. Phys. Soc. Jpn. **66**, 1066 (1997).
22. C. L. Kane and E. J. Mele, Phys. Rev. Lett. **93**, 197402 (2004).
23. C. D. Spataru, S. Ismail-Beigi, L. X. Benedict, and S. G. Louie, Phys. Rev. Lett. **92**, 077402 (2004).
24. V. Perebeinos, J. Tersoff, and P. Avouris, Phys. Rev. Lett. **92**, 257402 (2004).
25. H. Zhao and S. Mazumdar, Phys. Rev. Lett. **93**, 157402 (2004).
26. E. Chang, G. Bussi, A. Ruini, and E. Molinari, Phys. Rev. Lett. **92**, 196401 (2004).
27. F. Wang, G. Dukovic, L. E. Brus, and T. Heinz, Science **308**, 838 (2005).
28. J. Maultzsch, R. Pomraenke, S. Reich, E. Chang, D. Prezzi, A. Ruini, E. Molinari, M. S. Strano, C. Thomsen, and C. Lienau, Phys. Rev. B **72**, 241402(R) (2005).
29. Y. Ma, L. Valkunas, S. Bachilo, and G. Fleming, J. Phys. Chem. B **109**, 15671 (2005).
30. C. Fantini, A. Jorio, M. Souza, M. S. Strano, M. S. Dresselhaus, and M. A. Pimenta, Phys. Rev. Lett. **93**, 147406 (2004).
31. M. J. O'Connell, S. Sivaram, and S. K. Doorn, Phys. Rev. B **69**, 235415 (2004).
32. A. Hagen, M. Steiner, M. B. Raschke, C. Lienau, T. Hertel, H. Qian, A. J. Meixner, and A. Hartschuh, Phys. Rev. Lett. **95**, 197401 (2005).